ADVANCED INTELLIGENT SYSTEMS
Open Access
www.advintellsyst.com

Microendovascular Neural Recording from Cortical and Deep Vessels with High Precision and Minimal Invasiveness

*Takamitsu Iwata, Hajime Nakamura, Takafumi Uemura, Teppei Araki, Takaki Matsumura, Takaaki Abe, Toshikazu Nezu, Masatoshi Takagaki, Tomohiko Ozaki, Shinpei Miura, Ryohei Fukuma, Sam E. John, David B. Grayden, Haruhiko Kishima, Tsuyoshi Sekitani, and Takufumi Yanagisawa**

Intravascular electroencephalography (ivEEG) with microintravascular electrodes enhances neural monitoring, functional mapping, and brain–computer interfaces (BCIs), offering a minimally invasive approach to assess cortical activities; however, this approach remains unrealized. Current ivEEG methods using electrode-attached stents are limited to recording from large vessels, such as the superior sagittal sinus (SSS), restricting access to cortical regions essential for precise BCI control, such as those for hand and mouth movements. Here, ivEEG signals from small and soft cortical veins (CV-ivEEGs) in eight pigs using microintravascular electrodes are recorded, achieving higher resting-state signal power and greater spatial resolution of somatosensory evoked potentials (SEPs) compared to SSS-based ivEEG. Additionally, ivEEG recorded from deep veins clearly captures visual evoked potentials. Furthermore, comparisons between CV-ivEEG and electrocorticography (ECoG) using epidural and subdural electrodes in two pigs demonstrate that CV-ivEEG captures cortical SEPs comparable to ECoG. Targeted electrical stimulation via cortical vein electrodes induces specific contralateral muscle contractions in five anesthetized pigs, confirming selective motor-region stimulation with minimal invasiveness. The findings suggest that ivEEG with microintravascular electrodes is capable of accessing diverse cortical areas and capturing localized neural activity with high signal fidelity for minimally invasive cortical mapping and BCI.

1. Introduction

Less-invasive methods for recording intracranial electroencephalography (EEG) signals are essential for neural monitoring, functional mapping, and developing a clinically feasible brain–computer interface (BCI).[1,2] Intracranial EEG recording to search for the epileptic focus in patients with drug-resistant epilepsy requires less invasiveness and applicability to various brain regions, including the deep brain.[3] Stereotactic-EEG (SEEG) is a less-invasive intracranial EEG that can also be used for functional mapping without craniotomy, but SEEG requires approximately ten burr holes to be drilled in the skull.[4] Less-invasive and precise monitoring and functional mapping will improve the efficacy of epilepsy surgery. Moreover, various signal sources have been developed for invasive BCIs that can restore communication and motor functions in patients with severe paralysis[5] and monitor and consequently regulate various types of brain activity; however, there is no optimal method to record precise neural signals with minimal invasiveness.[6] Multiunit activity (MUA) obtained from the motor cortex related to the hand and mouth provides the most

T. Iwata, H. Nakamura, T. Matsumura, M. Takagaki, T. Ozaki, S. Miura, R. Fukuma, H. Kishima, T. Yanagisawa
Department of Neurosurgery, Graduate School of Medicine
The University of Osaka
Osaka 565-0871, Japan
E-mail: tyanagisawa@nsurg.med.osaka-u.ac.jp

T. Uemura, T. Araki, T. Abe, T. Nezu, T. Sekitani
SANKEN (The Institute of Scientific and Industrial Research)
The University of Osaka
Osaka 567-0047, Japan

T. Uemura, T. Araki, T. Sekitani
Advanced Photonics and Biosensing Open Innovation Laboratory
National Institute of Advanced Industrial Science and Technology (AIST)
Osaka 565-0871, Japan

R. Fukuma, T. Yanagisawa
Department of Neuroinformatics, Graduate School of Medicine
The University of Osaka
Osaka 565-0871, Japan

S. E. John, D. B. Grayden
Department of Biomedical Engineering and Graeme Clark Institute
The University of Melbourne
Melbourne 3010, Australia

The ORCID identification number(s) for the author(s) of this article can be found under https://doi.org/10.1002/aisy.202500487.

DOI: 10.1002/aisy.202500487

informative neural signals to ensure precise motor reconstruction of the hand[6,7] and clinically feasible communication at high speeds.[8,9] However, MUA-based BCIs are highly invasive and known for their low signal stability.[10] On the other hand, scalp EEG is noninvasive but provides less information than invasive signals do because of the limited signal-to-noise ratio and information transfer rate.[11] Compared to scalp EEG, electrocorticography (ECoG), which is less invasive than MUA, has attracted attention because it can achieve more feasible BCIs.[12] In particular, the use of high-density microelectrocorticography (μECoG) along with neural decoding based on deep neural networks and natural language processing has improved the performance of communication BCIs.[8,13,14] In addition, a system that uses epidural electrodes for recording signals stimulates the spinal cord of a patient with a spinal cord injury, enabling the patient to walk independently.[15] Although ECoG has demonstrated clinical feasibility, craniotomy is still required. There is a strong need for a minimally invasive technique that can stimulate various parts of the brain for functional mapping and provide stable and accurate information suitable for BCI and neural monitoring. However, this technique has not yet been demonstrated.

Intravascular EEG (ivEEG) is a minimally invasive technique for recording intracranial EEG signals without craniotomy.[16–18] Previous studies revealed that a stent with attached electrodes (called the "Stentrode," Synchron, USA) could be intravascularly implanted into the superior sagittal sinus (SSS) of sheep to record intracranial EEG signals.[17–19] ivEEG records somatosensory evoked potentials (SEPs) from the somatosensory cortex adjacent to the SSS.[19,20] Moreover, an ivEEG with a stent implanted in the SSS can be used to evaluate cortical activity related to foot movements in paralyzed patients and for BCI control of external devices.[21,22] However, ivEEG recordings using the Stentrode are limited to acquiring signals from the SSS, making it difficult to record motor cortical activity related to the hands and mouth, the main signal sources in current invasive BCIs.[6–8,12–14,23] Although other intravascular EEG methods have been proposed for epilepsy monitoring, accessible veins are limited to the sinus.[24,25] To use ivEEG to record various cortical and subcortical signals for use in BCIs and neural monitoring, smaller intravascular electrodes (called microintravascular electrodes) that can access the cortical veins and deep brain structures are needed.

Furthermore, the electrodes in the sinus, such as the SSS and cortex, are separated by the dura mater and the subdural and subarachnoid spaces.[26,27] Shorter distances between recording electrodes and the cortex are required for more precise and easily localized cortical signals.[28] Therefore, the ivEEG signals recorded from the SSS may have a lower signal-to-noise ratio (SNR) than the ECoG signals recorded by subdural electrodes on the cortical surface because of the distance from the cortex and the low-pass filtering due to the dura mater. The SNR of the ivEEG signals from the SSS has been reported to be similar to that of the ECoG signals acquired with epidural electrodes.[16,20] However, microintravascular electrodes positioned in cortical veins are closer to the cortex because the vessel walls are thin, potentially allowing them to provide higher-quality cortical signals recorded by the ECoG of cortical surface electrodes.

Here, we hypothesized that ivEEG recordings from electrodes in the cortical or deep veins could measure cortical activity with a higher SNR and identify areas related to motor and visual functions with higher spatial resolution than those from electrodes in the SSS and ECoG can. We used clinically available microguide wires as electrodes and implanted them into the cortical vein and deep veins of both miniature pigs and domestic pigs. We evaluated the efficacy of recording functional responses evoked by somatosensory and visual stimulation for mapping the functional areas of the sensorimotor and visual cortices.

2. Results

2.1. Endovascular Approach to the Intracranial Veins

We performed experiments on eight anesthetized pigs (five Clawn miniature pigs and three Zen-Noh Premium pigs; Supplementary Table 1). For all pigs, a linear incision was made in the skin of the left groin area, and 5 Fr and 8 Fr Super arrow-flex sheaths (Teleflex Medical Japan, Tokyo, Japan) were placed in the left femoral artery and vein, respectively. From the 5 Fr Super arrow-flex sheath, a 4 Fr Cerulean (Medikit, Tokyo, JAPAN) was inserted into the internal carotid artery, and venography was performed (**Figure 1**A and Supplementary Video 1). The diameters (mm) of the intracranial vessels of each pig are listed in Supplementary Table 1. From the 8 Fr Super arrow-flex sheath, an 8 Fr FUBUKI catheter (Asahi Intec, Aichi, JAPAN) was inserted into the cervical portion of the internal jugular vein. DeFrictor BULL (Medicos Hirata, Osaka, JAPAN) and Marathon (Medtronic, Minneapolis, MN, USA) microcatheters were then guided to the intracranial veins through the 8 Fr FUBUKI catheter. An ASAHI CHIKAI 10 (Asahi Intec, Nagoya, Aichi, JAPAN) was placed in the transverse sinus (TS), SSS, cortical veins, or deep veins through the microcatheters (Figure 1B and C and Supplementary Table 2). Notably, the tips of the guidewires for the SSS were slightly bent, with the curved part of the wire against the vessel walls.

2.2. Intravascular EEG of the SSS and CV

To record the ivEEG signals, we removed the polymer coating on the tip and end of each microguidewire (ASAHI CHIKAI 10 (Asahi Intec, Nagoya, Aichi, JAPAN)) and used the guidewires as microintravascular electrodes. First, we assessed the impedance between the two guidewires in the SSS by changing the length of the guidewires extending beyond the insulated catheter (DeFrictor BULL (Medicos Hirata, Osaka, Japan)). When both guidewires were placed inside the catheter, the impedance was greater than 50 kΩ (Figure 1D); however, the impedance decreased to less than 1 kΩ when at least 5 mm of both guidewires was exposed beyond the tip of the catheter (Figure 1D). Similarly, in saline solution, the impedance changed accordingly depending on the length of the exposed guidewire from the catheter (Supplementary Table 3). Afterward, we recorded the intravascular EEG signals with the tip 5–10 mm from the catheter.

First, for Pig A, two microintravascular electrodes were implanted into the SSS (Figure 1E), and then the same electrodes were guided to two CVs (Figure 1H) to measure the ivEEG signals in the SSS (SSS-ivEEG) and the cortical vein (CV-ivEEG). The mean duration from the start of the procedure to electrode

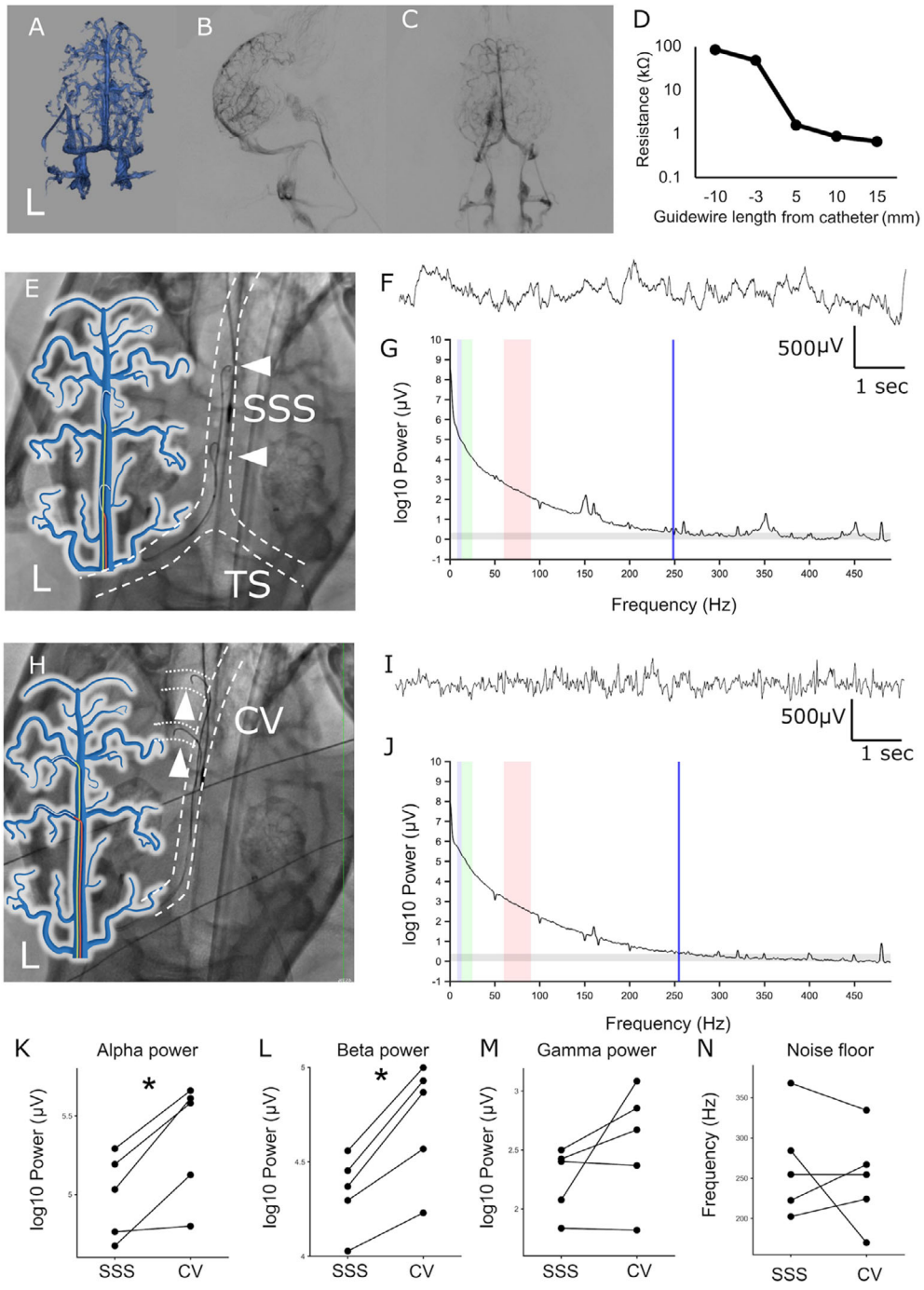

Figure 1. ivEEG measured with microintravascular electrodes implanted in the SSS and cortical vein. A–C) Angiography of miniature Pig A; 3D reconstruction image (A) and subtraction image of the lateral view (B) and AP view (C) of the venous phase. D) The impedance between two guide wires was assessed for various lengths of the guidewire beyond the catheter when the guidewires and catheter were inserted into Pig A. E) Venography and illustration of the two guidewires placed in the SSS (white arrowheads) of Pig A. The dashed line shows the SSS and TS. F) Representative waveforms of the SSS-ivEEG. G) Power spectrum density of the SSS-ivEEG. The blue, green, and red shaded areas represent the alpha, beta and gamma power bands, respectively. The gray band indicates the noise level. The blue line indicates the noise floor. H) Venography image and illustration of two guidewires placed in the left cortical veins (white arrowheads). The dashed line indicates the SSS and cortical veins. I) Representative waveforms of the CV-ivEEG. J) Power spectrum density of the CV-ivEEG. The blue, green and red areas represent the alpha, beta, and gamma power bands, respectively. The gray band indicates the noise level. The blue line indicates the noise floor. K–M) The PSDs of the SSS-ivEEG and CV-ivEEG data were compared across three frequency bands—alpha (K), beta (I), and gamma (M)—among five pigs. *$p<0.05$, paired *t*-test, Bonferroni corrected. N) Noise floors of SSS-ivEEG and CV-ivEEG for five pigs.

placement in the SSS was 127.6 (48.0) (mean (standard deviation (SD)), minutes, and an additional 61.9 (22.5) minutes were required to navigate the microintravascular electrodes into the CVs following completion of the SSS recording (Supplementary Table 4). In the SSS, the tips of the microintravascular electrodes were placed in contact with the right sinus wall. The electrode placement in the CV was carefully performed to avoid loading the vessel wall, but the time taken to place the electrode was 10 min (average for all subjects was 15 min). After the electrodes were placed, the SSS-ivEEG and CV-ivEEG data were recorded for 5 min without any stimulation (SSS-ivEEG, Figure 1F; CV-ivEEG, Figure 1I) while the pig was anesthetized. The ivEEG recordings were mostly stable, but sometimes, the baseline exceeded the recording range. After these artifact segments were removed, the power spectrum densities (PSDs) of the ivEEGs were assessed (Figure 1G and J; Methods). For both SSS-ivEEG and CV-ivEEG, the PSDs showed $1/f$ decay and exceeded the noise floor (based on the power in the 450–500 Hz range) up to the gamma range (SSS-ivEEG; 255 Hz, CV-ivEEG; 255 Hz). The PSDs of CV-ivEEG showed more signal power than those of SSS-ivEEG for Pig A (alpha: 52 dB (SSS-ivEEG), 56 dB (CV-ivEEG); beta: 46 dB (SSS-ivEEG), 50 dB (CV-ivEEG); and gamma: 25 dB (SSS-ivEEG), and 29 dB (CV-ivEEG)). Similarly, we recorded both CV-ivEEG and SSS-ivEEG for the other four pigs (Pigs B, C, D, and E). Among the five pigs, the PSDs showed significantly greater signal power for CV-ivEEG than for SSS-ivEEG for the alpha (8–13 Hz; $p = 0.0154$, $t(4) = -4.05$, $n = 5$, paired t-test, Bonferroni corrected) and beta (13–25 Hz; $p = 0.0031$, $t(4) = -6.39$, $n = 5$) frequencies but not gamma frequencies (60–90 Hz; $p = 0.1747$, $t(4) = -1.65$, $n = 5$) (Figure 1K, L, and M). Additionally, the noise floors of the SSS-ivEEG and CV-ivEEG recordings were not significantly different (mean: 266.4, 95% CI: 209.6–323.2 Hz for SSS-ivEEG; mean: 250.1, 95% CI: 197.3–302.8 Hz for CV-ivEEG; $p > 0.05$; paired t-test; $n = 5$; Figure 1N). Nonetheless, these results demonstrated that CV-ivEEG yielded larger signals for the alpha and beta ranges than did SSS-ivEEG.

2.3. SEP

To evaluate how CV-ivEEG can identify localized functional activities, SEPs were assessed (Methods). First, we recorded SSS-ivEEG signals via two microintravascular electrodes placed at the anterior and posterior parts of the SSS in Pig C. The tips of both microintravascular electrodes in the SSS were placed against the left wall of the SSS to record the ivEEG signals of the left hemisphere. The SEPs of the right and left median nerves of the pigs' forearms were subsequently compared (**Figure 2**A). The N20 amplitude was not significantly different between the two stimulation sides ($p > 0.05$, paired t-test, Bonferroni corrected; Figure 2B). Next, we recorded SEPs via CV-ivEEG from the microintravascular electrodes placed in the left anterior cortical vein and the posterior cortical vein of Pig C (Figure 2C). A clear N20 was observed in response to stimulation of the right median nerve; additionally, the N20 amplitude was significantly greater than that for stimulation of the left median nerve ($p < 0.05$, paired t-test, Bonferroni correction; Figure 2D). Lateralized SEPs were observed for three pigs via CV-ivEEG (Pigs D and E) but only one via SSS-ivEEG (Figure 2B, F, and J for SSS-ivEEG and D, H, and L for CV-ivEEG). These results suggest that CV-ivEEG is more sensitive to the anatomical location of electrodes than SSS-ivEEG is and can be used for functional mapping of the somatosensory cortex.

To compare the CV-ivEEG data with the ECoG data, we implanted epidural and subdural electrodes into two pigs (Pigs C and D) to collect CV-ivEEG data. For Pig C, we implanted epidural electrodes on the left frontal lobe close to the CV electrodes (Figure 2M). Conducting simultaneous CV-ivEEG and epidural ECoG recordings without stimulation revealed that the CV-ivEEG had a PSD similar to that of epidural ECoG (Figure 2N). In addition, simultaneous recordings with somatosensory stimulation revealed that the laterality of the SEP amplitude was greater in the CV-ivEEG recordings than in the epidural ECoG recordings (Figure 2O and P). Similarly, we implanted subdural electrodes close to the CV electrodes in Pig D (Figure 2Q). The PSD of the recordings during the resting state demonstrated that gamma power was significantly greater in the ECoG recordings than in the CV-ivEEG recordings (Figure 2R). On the other hand, the laterality of SEPs from CV-ivEEG and ECoG recordings was similar (Figure 2S and T), although the amplitude of CV-ivEEG SEPs was greater than that of ECoG SEPs. These results demonstrate that CV-ivEEG records cortical responses with similar signal power to those of the ECoG and sometimes assesses functional localization better than ECoG recordings do.

To further assess functional localization on the basis of the phase reversal of SEPs, we implanted three guidewires in the SSS and cortical veins of two pigs (Pigs F and G) (**Figure 3**A and C). The N20 of the SEP was compared between two adjacent guidewires. The phase reversal of N20 was confirmed for both pigs (Figure 3B and D). These results indicate that ivEEG modalities, including CV-ivEEG, can map the sensorimotor cortex by measuring the phase reversal of SEPs.

2.4. Motor Evoked Potentials can be Measured through the Cortical Intravascular System

For five pigs (Pigs A, B, C, F, and H), electrical stimulation was applied through the microintravascular electrode to identify motor cortical responses. The muscle responses were assessed by measuring motor-evoked potentials (MEPs) with electrodes inserted into the muscles of the pigs' lips and shoulders and confirmed by observing muscle contraction. For Pigs A and B, reproducible localized muscle responses to electrical stimulation with electrodes implanted in the SSS were not observed. For Pig A, electrical stimulation with a biphasic pulse of 50 Hz between the electrodes at the left anterior CV and SSS induced muscle contraction of the right shoulder (Figure 3E). On the other hand, the same stimulation at the left anterior CV and left posterior CV induced muscle contraction of the right upper lip (Figure 3F). In addition, the short electrical stimulation of five biphasic pulses of 500 Hz in the same electrode pairs induced a clear motor-evoked response recorded by the electrodes at the right upper lip (Figure 3G and Supplementary Video 2). Similarly, among the other four pigs, cortical stimulation of the microintravascular electrode induced muscle twitches on the contralateral face and shoulder (Figure 3H and I). Notably, in Pig H, stimulation of the electrodes

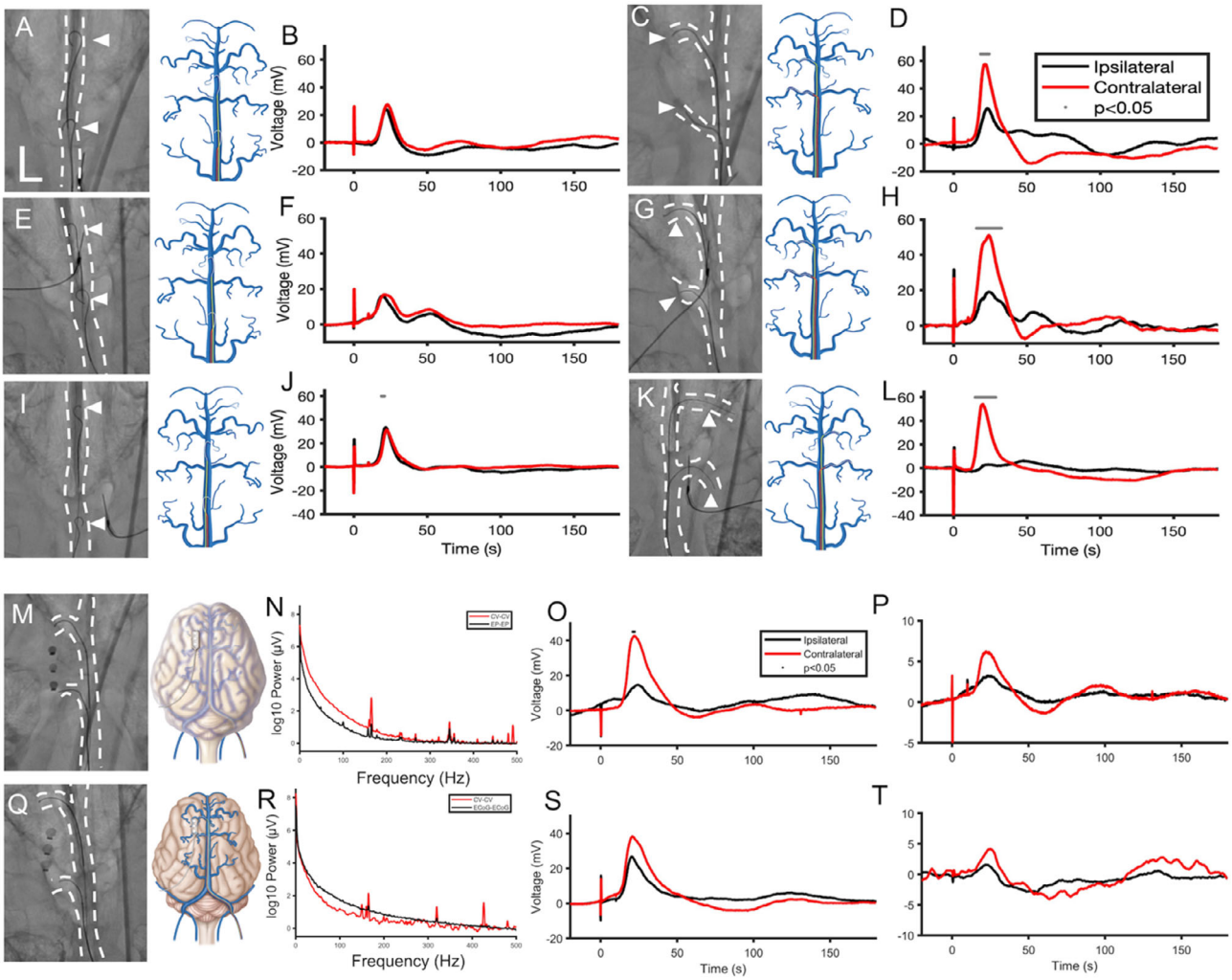

Figure 2. SEPs of SSS-ivEEG, CV-ivEEG, and ECoG. A) Venography and illustration of SSS-ivEEG in Pig C. The electrodes were attached to the right wall of the SSS. B) SEP recorded by SSS-ivEEG in Pig C. The red and black lines correspond to the responses to stimulation of the contralateral (left) and ipsilateral (right) forearms of the pig. C) Venography image and illustration of CV-ivEEG in Pig C. The electrodes were placed in the left cortical veins. D) SEP recorded by CV-ivEEG in Pig C. The red and black lines correspond to the response stimulated to the contralateral (right) and ipsilateral (left) forearms of the pig. The gray dots indicate the times at which the amplitudes of contralateral and ipsilateral stimulation were significantly different ($p < 0.05$, paired t-test, Bonferroni corrected). E) Venography and illustration of SSS-ivEEG of Pig D. F) SEP of SSS-ivEEG in Pig D. G) Venography and illustration of CV-ivEEG of Pig D. H) SEP of CV-ivEEG in Pig D. I) Venography and illustration of SSS-ivEEG of Pig E. J) SEP of SSS-ivEEG in Pig E. K) Venography and illustration of CV-ivEEG of Pig E. L) SEP of CV-ivEEG in Pig E. M) X-ray image and illustration of implanted electrodes of Pig C. N) PSDs of CV-ivEEG and epidural ECoG during the resting state. O,P) SEPs resulting from stimulation of the forearms contralateral and ipsilateral to the implanted electrodes in the O) CV and P) epidural spaces. The black dots indicate time points when the amplitudes of contralateral and ipsilateral stimulation were significantly different ($p < 0.05$, paired t-test, Bonferroni corrected). Q) X-ray image and illustration of implanted electrodes of Pig D. R) PSDs of CV-ivEEG and subdural ECoG during the resting state. S,T) SEPs resulting from stimulation of the forearms contralateral and ipsilateral to the implanted electrodes in the (S) CV and (T) subdural space.

at the frontal pole induced no muscle contraction, although stimulation of the middle part of the brain induced contralateral muscle contraction. These findings suggest that CV electrodes can identify the motor cortex by assessing localized MEP responses.

2.5. Visual Evoked Potentials Measured through Deep Veins

Visual evoked potentials (VEPs) were recorded via ivEEG from the deep vein. ivEEG signals were recorded between two guidewires placed in the internal cerebral vein (ICV) and the TS (**Figure 4**A). In addition, ivEEG signals were recorded between the microintravascular electrode at the TS and the scalp electrode attached to the back of the pig's head (Oz). The following light stimulation was applied to both eyes: intensity 2000 lux, frequency 3 Hz, and duration 20 ms. Then, the VEP was measured. The results revealed a clear peak potential of ≈40 ms in both cases, but the amplitude of the intravascular EEG was greater with the ICV-TS than with the Oz-TS, with less noise (Figure 4B and C).

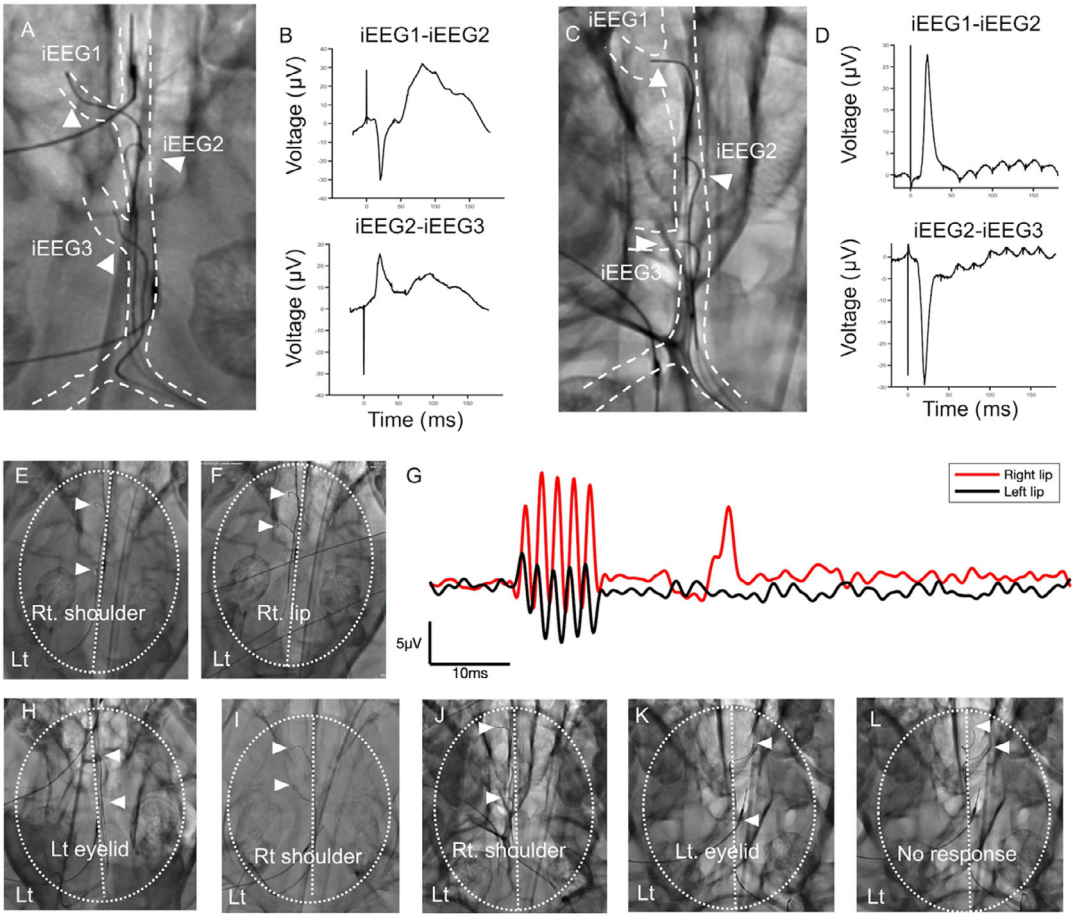

Figure 3. Functional localization observed by ivEEGs. A) X-ray of the micro- and intravascular electrodes of pig G. B) SEPs from stimulation of the forearms contralateral (red) and ipsilateral (black) to the implanted electrodes (ivEEG1-ivEEG2 and ivEEG2-ivEEG3). C) X-ray of the micro- and intravascular electrodes of pig F. D) SEPs resulting from stimulation of the forearms contralateral to the implanted electrodes (ivEEG1-ivEEG2 and ivEEG2-ivEEG3). E) X-ray image showing the location of the electrodes (white arrowheads) in Pig A. The white dotted line shows the skull and centerline of the pig's head. Stimulation at 50 Hz on the electrodes induced muscle contractions on the right shoulder of the pig. F) Electrode location of Pig A. Electrical stimulation at 500 Hz induced muscle contraction of the right lip. G) Electromyogram recorded from the right (red) and left (black) sides of the lip of the pig. H) Electrical stimulation at 50 Hz (white arrowheads) induced muscle contractions on the left side of the face of Pig B. I) Electrical stimulation at 50 Hz induced movements of the right shoulder in Pig C. J) Stimulation at 50 Hz induced right shoulder movements in Pig F. K) Stimulation at 50 Hz induced movements of the left eye lid in Pig H. L) Stimulation at 50 Hz did not induce any muscle contractions in Pig H.

2.6. Safety Assessment of Intravascular Cortical Electrodes

We safely placed microguidewires (CHIKAI10) into the cortical and deep veins of eight pigs. During the insertion of the micro guidewires, we spent 5–6 h recording ivEEG data while frequently repositioning the electrodes. However, we observed no obvious extravasation or any other finding that might suggest vascular injury. In addition, some pigs with microguidewires implanted in the CV and SSS were craniotomized, but we did not observe any obvious vascular injuries, such as subarachnoid hemorrhage, indicating that microguidewires can be safely used to record ivEEG data from the cortical and deep veins. In general, the vessel diameters of miniature pigs are small: 1.9 (0.5) mm for the SSS, 0.5 (0.29) mm for the CV, and 1.4 (0.2) mm for the internal jugular vein (Supplementary Table 2). Notably, the size of the SSS in miniature pigs corresponds to the size of the cortical vein in humans.[29] These results in miniature pigs suggest that the microendovascular system can be used to safely access the cortical vein in the human brain and measure intravascular EEGs.

3. Discussion

This study demonstrated that ivEEG recorded by microguidewires (microintravascular electrodes) in the cortical vein and deep vein can measure functional cortical responses with amplitudes that are comparable and sometimes larger than those of ECoG, and that various cortical regions can be accessed for functional mapping less invasively. Compared with those of SSS-ivEEG, the CV-ivEEG PSDs demonstrated greater signal power in the alpha and beta ranges. Compared with those measured with SSS-ivEEG, the SEPs measured by CV-ivEEG demonstrated greater contrast to the stimulated side than those measured with SSS-ivEEG did, suggesting that CV-ivEEG can

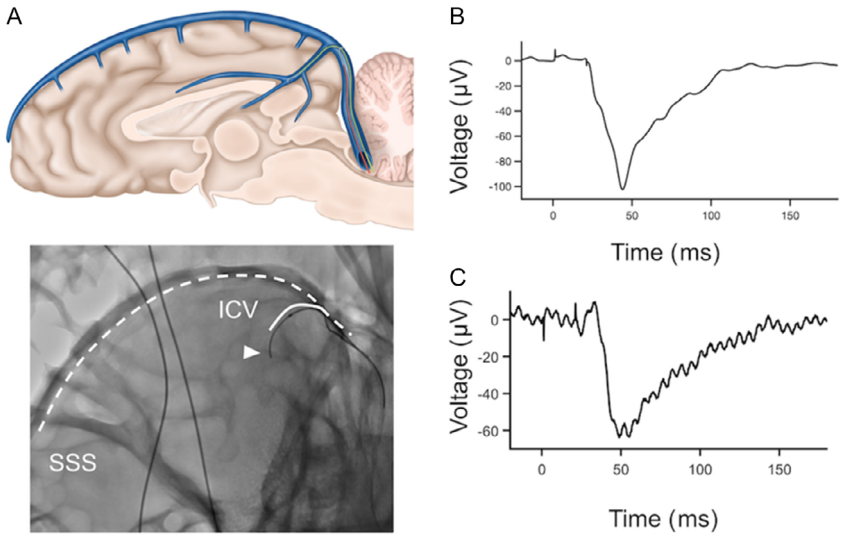

Figure 4. VEPs recorded by ivEEG in the ICV. A) Illustration (upper panel) and X-ray image (lower panel) of the implanted electrodes in Pig F. B,C) VEPs recorded by microintravascular electrodes between the (B) ICV and TS and between the (C) TS and Oz.

detect spatially localized responses. Using microintravascular electrodes, both the MEP and the phase reversal of N20 could be identified, facilitating mapping of the motor cortex. In addition, VEPs can be measured from the ICV or SSS via microintravascular electrodes, confirming their ability to access various brain regions that are difficult to record with subdural electrodes. These results demonstrated that ivEEG can yield high SNRs and area-specific recordings of intracranial EEGs with minimal invasiveness when an electrode is used to access the cortical and deep veins.

Our results suggest that CV-ivEEG has a greater SNR than SSS-ivEEG does in terms of both PSD and SEPs. In addition, the SNR of CV-ivEEG was comparable to that of epidural and subdural ECoGs. These results are consistent with those of previous studies showing that SSS-ivEEG has a similar SNR to epidural ECoG and a smaller SNR than subdural ECoG does.[19] The SNR of EEG is affected by both the distance of the electrode from the cortex and the intervening tissue; in the SSS, the dura mater and cerebral fluid act as low-pass filters, attenuating high-frequency band activity. Because the superficial cerebral vein has thin vascular walls and is close to the cortex, CV-ivEEG provides a higher SNR than SSS-ivEEG does. Therefore, compared to electrodes implanted in the SSS, electrodes implanted in the CV seem to provide a higher SNR on EEG.

Using a microguidewire to access cortical and deep vessels, cortical region-specific signals can be obtained. For intravascular EEG in the SSS, it was also possible to measure hemispheric-specific SEPs depending on whether the electrode was placed on the left or right wall. However, obtaining localized muscle responses with electrical stimulation with electrodes implanted in the SSS was difficult. Nonetheless, electrical stimulation from wires in the CVs was shown to allow cortical area-specific motor cortical stimulation. In particular, the mouth region of pigs can be selectively stimulated, suggesting that the CV can be used to measure motor cortex activity in the mouth, which is important for speech BCIs.[8,13,14] Notably, a clear correspondence between pigs and humans is difficult to establish because of differences in the functional arrangement of the sensorimotor cortex.[30,31] VEPs were also measured in deep blood vessels. Visual responses can also be used for communication BCIs.[32] It has been shown that function-specific activity can be obtained with high accuracy by performing ivEEG with a microguidewire. Furthermore, these findings suggest that signals can be acquired from deep structures, such as the brainstem and basal ganglia, as well as from superficial regions such as the SSS and TS.

Although our findings demonstrate promising potential for the clinical application of microintravascular EEG, this study was conducted as an acute experiment in pigs, and several important considerations must be addressed before translating to human use. Notably, the diameter of the SSS in humans at the Bregma level is ≈6.5 (2.8) mm, whereas in our miniature pigs it was only 1.9 (0.5) mm (Supplementary Table 2), indicating that the porcine venous anatomy is substantially smaller.[33] Despite these anatomical limitations, successful endovascular access to CVs in pigs suggests that navigation within larger human cortical veins should be technically feasible.

However, owing to the acute nature of our study, we were unable to assess chronic implantation-related phenomena, such as endothelialization, which has been identified as a key feature of the Stentrode system that enables long-term integration with the vessel wall and potentially reduces thrombosis risk.[2] For future clinical translation, it will be necessary to evaluate whether the long-term implantation of microintravascular electrodes induces endothelialization and how such vascular responses affect the signal stability, thrombogenicity, and patency of cortical veins. These considerations are critical not only for ensuring safety and functionality but also for guiding the design of next-generation intravascular devices. Future electrodes should be optimized for mechanical flexibility, thrombogenic potential, and chronic electrical stability to achieve reliable long-term implantation in the human brain.

This study has several limitations. Since this study was conducted as an acute-phase experiment, we were unable to assess

the long-term stability and safety of CV-ivEEG. However, no major adverse events occurred during the experiments. Further work is needed on risks such as thrombosis due to long-term implantation. Additionally, in this study, CHIKAI10 was used for CV-ivEEG measurements; however, CHIKAI10 was not originally intended for this application. While the resistance values of the electrodes were sufficient for the EEG recordings, future work should focus on the development of dedicated electrodes that impose minimal strain on cortical veins while ensuring accurate measurement.

4. Conclusion

Our results suggest that ivEEG using microintravascular electrodes can access diverse cortical areas and capture localized neural activity with high signal accuracy. This minimally invasive technique enables precise cortical mapping via the cortical and deep veins, representing a significant advancement in neural monitoring and neuromodulation in both research and clinical contexts.

5. Experimental Section

Study Design and Approval: All the surgical and experimental procedures were performed at the Fukushima Medical Device Development and Support Center. The research protocol was approved by the Institutional Review Board (approval no. 04-073-000) and included an evaluation of approaches for accessing the brain surface and deep veins in pigs with a catheter, an evaluation of microguidewire-based EEG measurements from within the vessels, and a comparison of the acquired EEG signals with those acquired by ECoG. The quality of the EEGs was assessed in terms of the measured SEPs, MEPs, and VEPs. Unless otherwise specified, significant differences were assessed using paired *t*-test. This study used observational data, and data analysis was performed using MATLAB 2017b.

Animal and Experimental Information: The study was observational and not an intervention study; therefore, randomization was not performed. The smallest number of animals required to demonstrate feasibility was used in accordance with the policy of the institutional animal ethics committee. The experiments were conducted on the female pigs weighing ≈40 kg. The animal was selected by an experimenter independent of the measurement process. This experimenter was not informed of the procedures or measurement details and selected animals based on their condition. Healthy eight pigs (16.5 months old, 43.1 kg) were subjected to experimental procedures (Supplementary Table 1). The sample size of five subjects was determined based on an a priori power analysis assuming a strong effect size. Specifically, we assumed a large effect size (Cohen's $d = 1.2$) for the paired *t*-test, with an alpha level of 0.05 and power of 0.8, which indicated that a minimum of five subjects would be sufficient to detect statistically significant differences. The procedure was performed under general anesthesia, which was induced with isoflurane. General anesthesia was subsequently maintained with continuous infusions of propofol [2 mg kg^{-1} h^{-1}] and dexmedetomidine [0.5 mg kg^{-1} h^{-1}]). Additional doses of propofol or dexmedetomidine were administered as needed when body movements occurred. The intracranial vascular anatomy of pigs was similar to that of humans, with the cortical vein flowing into the SSS and merging with the straight sinus from the inferior sagittal sinus. However, it differed from humans in that the transverse sinus drained into the vertebral venous plexus and internal jugular venous system via the sigmoid sinus.

Microintravascular Electrode Placement: Cerebral angiography was performed at the Fukushima Medical Device Development and Support Center. Groin puncture was performed with a cut-down procedure under ultrasound guidance, and 5 and 8 Fr Super arrow-flex sheaths (Teleflex Medical Japan, Tokyo, Japan) were inserted into the femoral artery and vein, respectively. Heparin was administered at a dose of 100 international units (IU)/kg via an intravenous catheter placed in the ear vein, and an activated coagulation time longer than 250 s was maintained during the procedure. Digital subtraction angiography was performed with an INFX-800C (Canon Medical Systems, Tochigi, Japan); specifically, 3 mL of iopamidol was injected at 0.5 mL s^{-1} as contrast medium via a 4 Fr Cerulean catheter placed in the internal carotid artery. Additionally, 3D rotational angiography/venography was performed to evaluate the precise vascular architecture, with 5 mL of contrast medium injected at a rate of 0.5 mL s^{-1}.

To access cortical veins from the femoral vein, an 8 Fr FUBUKI catheter (Asahi Intec, Aichi, JAPAN) was introduced into the internal carotid vein via 8 Fr Super arrow-flex sheaths using a coaxial catheter and a 0.035 inch guidewire. The microcatheters were maneuvered into the intracranial veins (sigmoid sinus, transverse sinus, superior sagittal sinus, internal cerebral vein, and cortical veins) through the jugular bulb using a 0.010 inch guidewire. In this procedure, roadmap navigation under the ideal projection was needed to clearly identify the venous route.

After the microcatheter reached the target vessels, a 0.010 inch guidewire was pulled back, and then the ivEEG electrodes were positioned at the target vessels using the microcatheter. In the venous sinus, the 5 mm tip of the wire was bent into a J shape to make contact with the vessel wall. However, the diameter of the cortical veins was ≈1 mm; therefore, high-definition angiographic equipment and delicate catheter guidance techniques were essential, and the tip was not bent in the cortical veins.

EEG Measurement: Scalp and intracranial EEGs were measured via a Power Lab 4/26 with an FE232 Dual Bio AMP (ADInstruments, Dunedin, New Zealand). The recordings were sampled at 10 000 Hz. When the intracranial EEG was measured, an alligator clip was attached to the tip of the CHIKAI 10 and connected to the EEG system. The end-to-end resistance of CHIKAI 10 was sufficiently low, ≈ 40 Ω. EEG recordings were obtained without applying a low-pass filter, but a high-pass filter with a cut-off frequency of 0.1 Hz was used. To remove the influence of body movement due to breathing, the wires of the recording electrodes were fixed to the bed or the floor. The ground electrode was placed on the skin of the neck or shoulder.

The Fz electrode was inserted into the nasal root, and the Cz electrode was inserted into the midline of the cranium; placement was confirmed in the frontal fluoroscopy image.

The impedance measurements were made at a frequency of 100 Hz via an LCR meter IM3590 (HIOKI E.E. Co., Nagano, JAPAN) or LCR-916 (GW Instek, TAIWAN). When the impedance was measured, the distance the guidewire protruded from the catheter tip was visually assessed on the radiographic fluoroscopic image.

Power Spectral Density: The recorded signals were segmented into 2-s epochs, and epochs with signals exceeding the recording limits were excluded from further analysis. To remove power line noise, a 50 Hz notch filter and 0.5–500 Hz bandpass filter were applied. The noise of each electrode was estimated using the median spectral power between 455 and 495 Hz of each recording electrode. This frequency band was chosen because it is the highest-frequency band located below the Nyquist frequency and does not include any harmonics of the 50-Hz line noise. The noise floor was defined as the frequency at which the power first dropped below the upper limit of noise (mean + 1 SD). Since ECoG power spectra were not normally distributed and showed considerable variability within subjects, the mean power spectrum was normalized to the mean noise power and log-transformed. We compared the alpha, beta, and gamma frequencies, as well as the noise floors derived from the signal power of the SSS-ivEEG and CV-ivEEG recordings. These computations were carried out using MATLAB 2017b.

SEP: SEPs were measured in a cohort of five pigs using microivEEG. SEPs were recorded under general anesthesia. A modular stimulator NS-101 (UNIQUE MEDICAL, Tokyo, Japan) was used to generate a stimulation current. Needle electrodes were inserted into the median nerve of the bilateral forelegs for bipolar electrical stimulation.[34,35] Stimulations with an amplitude of 25–30 mA, a pulse width of 0.2 s, and a stimulus frequency of 4.3 Hz were applied and repeated 200 times. The stimulation amplitude was changed for each experimental condition. Neural signals were bandpass filtered with a 0.1 Hz high-pass filter. Averaged SEP

waveforms were normalized by the mean of the baseline signals (from −20 to 0 ms).

MEP: An alligator clip was attached to the tip of the CHIKAI 10, and a modular stimulator NS-101 (UNIQUE MEDICAL, Tokyo, Japan) was used for stimulation. Stimulation was conducted at a frequency of 50 Hz, with a 20 mA current, a pulse width of 0.5 ms, and a duration of 3 s. Muscle contraction was visually detected before stimulation at 500 Hz (20 mA, pulse width of 1 md, biphasic, in five trains).[34] In this case, the MEP was measured by inserting a needle electrode into the shoulder and upper lip muscles using a Power Lab 4/26 system with a FE232 Dual Bio AMP (ADInstruments, Dunedin, New Zealand).

VEP: Stimulations were conducted using an LED light stimulation device (LFS-101 III Unique Medical, Tokyo, Japan) in a lighting room. LED pads were applied over the eyelids of both closed eyes. The stimulation conditions were 20 000 lux, 20 ms stimulation duration, 3 Hz stimulation frequency, and 200 repetitions.[36]

ECoG Recording: The electrocorticography electrodes consisted of three pole electrodes mounted on a silicon sheet measuring 5 mm by 15 mm (Unique Medical, Tokyo, Japan). Each electrode had 3 mm-diameter contacts, and the electrodes were placed 5 mm apart. The pigs were placed in a prone position for the placement of the electrocorticography electrodes. The appropriate position for craniotomy was determined via X-ray fluoroscopy. A skin incision was then made, part of the skull was removed using a drill, and the dura mater was exposed. A linear incision was carefully made in the dura mater, allowing for the placement of an electrocorticography electrode directly on the surface of the brain.

Supporting Information

Supporting Information is available from the Wiley Online Library or from the author.

Acknowledgements

The authors gratefully thank all the staff of the Fukushima Medical Device Development and Support Center for their support in this research.

Conflict of Interest

The authors declare no conflict of interest.

Author Contributions

Takamitsu Iwata: data curation (lead); investigation (lead); visualization (lead); writing—original draft (equal); writing—review and editing (lead). **Hajime Nakamura**: data curation (lead); funding acquisition (equal); investigation (lead); methodology (lead); project administration (equal); writing—review and editing (equal). **Takafumi Uemura**: data curation (equal); investigation (equal); writing—review and editing (equal). **Teppei Araki**: data curation (supporting); investigation (supporting); resources (supporting); writing—review and editing (supporting). **Takaki Matsumura**: data curation (supporting); investigation (supporting); writing review and editing (supporting). **Takaaki Abe**: data curation (supporting); investigation (supporting); writing—review and editing (supporting). **Toshikazu Nezu**: data curation (supporting); investigation (supporting); writing—review and editing (supporting). **Masatoshi Takagaki**: data curation (supporting); investigation (supporting); writing review and editing (supporting). **Tomohiko Ozaki**: data curation (supporting); investigation (supporting); writing—review and editing (supporting). **Shinpei Miura**: data curation (supporting); investigation (supporting); writing—review and editing (supporting). **Ryohei Fukuma**: investigation (supporting); methodology (equal); resources (equal); writing—review and editing (supporting). **Sam E. John**: writing—review and editing (supporting). **David B. Grayden**: writing—review and editing (supporting). **Haruhiko Kishima**: writing—review and editing (supporting). **Tsuyoshi Sekitani**: conceptualization (equal); data curation (supporting); funding acquisition (equal); investigation (equal); methodology (equal); resources (equal); supervision (equal); writing—review and editing (equal). **Takafumi Yanagisawa**: conceptualization (lead); data curation (supporting); formal analysis (supporting); funding acquisition (lead); investigation (lead); project administration (lead); supervision (lead); validation (lead); writing—original draft (lead). **Takamitsu Iwata**, **Hajime Nakamura**, and **Takafumi Uemura** contributed equally to this work.

Data Availability Statement

The data that support the findings of this study are available in the supplementary material of this article.

Keywords

brain–computer interfaces, cortical veins, epilepsy, intravascular electroencephalography, minimal invasiveness

Received: April 30, 2025
Revised: July 29, 2025
Published online:

[1] M. Carè, M. Chiappalone, V. R. Cota, *Front. Neurosci.* **2024**, *18*, 1363128.
[2] S. E. John, D. B. Grayden, T. Yanagisawa, *Expert Rev. Med. Devices* **2019**, *16*, 841.
[3] B. E. Youngerman, F. A. Khan, G. M. McKhann, *Neuropsychiatr. Dis. Treat.* **2019**, *15*, 1701.
[4] K. M. Grande, S. K. Z. Ihnen, R. Arya, *Front. Hum. Neurosci.* **2020**, *14*, 611291.
[5] J. F. M. Brannigan, K. Liyanage, H. L. Horsfall, L. Bashford, W. Muirhead, A. Fry, *J. Neural Eng.* **2024**, *21*, 061005.
[6] S. N. Flesher, J. E. Downey, J. M. Weiss, C. L. Hughes, A. J. Herrera, E. C. Tyler-Kabara, M. L. Boninger, J. L. Collinger, R. A. Gaunt, *Science* **2021**, *372*, 831.
[7] F. R. Willett, D. T. Avansino, L. R. Hochberg, J. M. Henderson, K. V. Shenoy, *Nature* **2021**, *593*, 249.
[8] S. L. Metzger, K. T. Littlejohn, A. B. Silva, D. A. Moses, M. P. Seaton, R. Wang, M. E. Dougherty, J. R. Liu, P. Wu, M. A. Berger, I. Zhuravleva, A. Tu-Chan, K. Ganguly, G. K. Anumanchipalli, E. F. Chang, *Nature* **2023**, *620*, 1037.
[9] N. S. Card, M. Wairagkar, C. Iacobacci, X. Hou, T. Singer-Clark, F. R. Willett, E. M. Kunz, C. Fan, M. Vahdati Nia, D. R. Deo, A. Srinivasan, E. Y. Choi, M. F. Glasser, L. R. Hochberg, J. M. Henderson, K. Shahlaie, S. D. Stavisky, D. M. Brandman, *N. Engl. J. Med.* **2024**, *391*, 609.
[10] E. G. M. Pels, E. J. Aarnoutse, S. Leinders, Z. V. Freudenburg, M. P. Branco, B. H. van der Vijgh, T. J. Snijders, T. Denison, M. J. Vansteensel, N. F. Ramsey, *Clin. Neurophysiol.* **2019**, *130*, 1798.
[11] B. J. Edelman, S. Zhang, G. Schalk, P. Brunner, G. Müller-Putz, C. Guan, B. He, *IEEE Rev. Biomed. Eng.* **2025**, *18*, 26.
[12] M. J. Vansteensel, E. G. M. Pels, M. G. Bleichner, M. P. Branco, T. Denison, Z. V. Freudenburg, P. Gosselaar, S. Leinders, T. H. Ottens, M. A. Van Den Boom, P. C. Van Rijen, E. J. Aarnoutse, N. F. Ramsey, *N. Engl. J. Med.* **2016**, *375*, 2060.
[13] X. Chen, R. Wang, A. Khalilian-Gourtani, L. Yu, P. Dugan, D. Friedman, W. Doyle, O. Devinsky, Y. Wang, A. Flinker, *Nat. Mach. Intell.* **2024**, *6*, 467.
[14] D. A. Moses, S. L. Metzger, J. R. Liu, G. K. Anumanchipalli, J. G. Makin, P. F. Sun, J. Chartier, M. E. Dougherty, P. M. Liu,

G. M. Abrams, A. Tu-Chan, K. Ganguly, E. F. Chang, *N. Engl. J. Med.* **2021**, *385*, 217.

[15] H. Lorach, A. Galvez, V. Spagnolo, F. Martel, S. Karakas, N. Intering, M. Vat, O. Faivre, C. Harte, S. Komi, J. Ravier, T. Collin, L. Coquoz, I. Sakr, E. Baaklini, S. D. Hernandez-Charpak, G. Dumont, R. Buschman, N. Buse, T. Denison, I. van Nes, L. Asboth, A. Watrin, L. Struber, F. Sauter-Starace, L. Langar, V. Auboiroux, S. Carda, S. Chabardes, T. Aksenova, et al., *Nature* **2023**, *618*, 126.

[16] T. J. Oxley, N. L. Opie, S. E. John, G. S. Rind, S. M. Ronayne, T. L. Wheeler, J. W. Judy, A. J. McDonald, A. Dornom, T. J. H. Lovell, C. Steward, D. J. Garrett, B. A. Moffat, E. H. Lui, N. Yassi, B. C. V. Campbell, Y. T. Wong, K. E. Fox, E. S. Nurse, I. E. Bennett, S. H. Bauquier, K. A. Liyanage, N. R. van der Nagel, P. Perucca, A. Ahnood, K. P. Gill, B. Yan, L. Churilov, C. R. French, et al., *Nat Biotechnol* **2016**, *34*, 320.

[17] R. D. Penn, S. K. Hilal, W. J. Michelsen, E. S. Goldensohn, J. Driller, *J. Neurosurg.* **1973**, *38*, 239.

[18] B. D. He, M. Ebrahimi, L. Palafox, L. Srinivasan, *J. Neural Eng.* **2016**, *13*, 016016.

[19] S. E. John, N. L. Opie, Y. T. Wong, G. S. Rind, S. M. Ronayne, G. Gerboni, S. H. Bauquier, T. J. O'Brien, C. N. May, D. B. Grayden, T. J. Oxley, *Sci. Rep.* **2018**, *8*, 8427.

[20] M. R. Bower, M. Stead, J. J. Van Gompel, R. S. Bower, V. Sulc, S. J. Asirvatham, G. A. Worrell, *J. Neurosci. Methods* **2013**, *214*, 21.

[21] T. J. Oxley, P. E. Yoo, G. S. Rind, S. M. Ronayne, C. M. S. Lee, C. Bird, V. Hampshire, R. P. Sharma, A. Morokoff, D. L. Williams, C. MacIsaac, M. E. Howard, L. Irving, I. Vrljic, C. Williams, S. E. John, F. Weissenborn, M. Dazenko, A. H. Balabanski, D. Friedenberg, A. N. Burkitt, Y. T. Wong, K. J. Drummond, P. Desmond, D. Weber, T. Denison, L. R. Hochberg, S. Mathers, T. J. O'Brien, C. N. May, J. Mocco, D. B. Grayden, B. C. V. Campbell, P. Mitchell, N. L. Opie, *J. Neurointerv. Surg.* **2021**, *13*, 102.

[22] P. Mitchell, S. C. M. Lee, P. E. Yoo, A. Morokoff, R. P. Sharma, D. L. Williams, C. MacIsaac, M. E. Howard, L. Irving, I. Vrljic, C. Williams, S. Bush, A. H. Balabanski, K. J. Drummond, P. Desmond, D. Weber, T. Denison, S. Mathers, T. J. O'Brien, J. Mocco, D. B. Grayden, D. S. Liebeskind, N. L. Opie, T. J. Oxley, B. C. V. Campbell, *JAMA Neurol.* **2023**, *80*, 270.

[23] F. R. Willett, E. M. Kunz, C. Fan, D. T. Avansino, G. H. Wilson, E. Y. Choi, F. Kamdar, M. F. Glasser, L. R. Hochberg, S. Druckmann, K. V. Shenoy, J. M. Henderson, *Nature* **2023**, *620*, 1031.

[24] A. Fujimoto, Y. Matsumaru, Y. Masuda, A. Marushima, H. Hosoo, K. Araki, E. Ishikawa, *Brain Sci.* **2022**, *12*, 309.

[25] N. Mikuni, A. Ikeda, K. Murao, K. Terada, I. Nakahara, W. Taki, H. Kikuchi, H. Shibasaki, *Epilepsia* **1997**, *38*, 472.

[26] J. Moini, P. Piran, *Functional And Clinical Neuroanatomy*, Elsevier **2020**, pp. 95–129.

[27] E. Egemen, I. Solaroglu, *Primer On Cerebrovascular Diseases*, Elsevier **2017**, pp. 32–36.

[28] A. Zhang, E. T. Mandeville, L. Xu, C. M. Stary, E. H. Lo, C. M. Lieber, *Science* **2023**, *381*, 306.

[29] S. Tsutsumi, H. Ono, H. Ishii, *Surg. Radiol. Anat.* **2021**, *43*, 235.

[30] P. del Cerro, Á. Rodríguez-De-Lope, J. E. Collazos-Castro, *Front. Neuroanat.* **2021**, *15*, 748050.

[31] S. Desantis, S. Minervini, L. Zallocco, B. Cozzi, A. Pirone, *Animals* **2021**, *11*, 2019.

[32] R. Fukuma, T. Yanagisawa, S. Nishimoto, H. Sugano, K. Tamura, S. Yamamoto, Y. Iimura, Y. Fujita, S. Oshino, N. Tani, N. Koide–Majima, Y. Kamitani, H. Kishima, *Commun. Biol.* **2022**, *5*, 214.

[33] D. Z. Oberman, N. N. Rabelo, J. L. A. Correa, P. Ajler, *Surg. Neurol. Int.* **2020**, *11*, 309.

[34] S. Maier, U. Goebel, S. Krause, C. Benk, M. A. Schick, H. Buerkle, F. Beyersdorf, F. A. Kari, J. Wollborn, *PLoS One* **2018**, *13*, e0205410.

[35] G. L. Hoareau, A. Peters, D. Hilgart, M. Iversen, G. Clark, M. Zabriskie, V. Rieke, C. Floyd, L. Shah, *Lab. Anim. Res.* **2022**, *38*, 9.

[36] R. A. Oeur, M. Palaniswamy, M. Ha, M. Fernández Corazza, S. S. Margulies, *Physiol. Meas.* **2023**, *44*, 025006.